Quaternary Research (2025), 1–11
doi:10.1017/qua.2025.20

Research Article

A late Pleistocene glacial maximum during MIS 3 in the Chersky Mountains, central northeast Siberia

Jesper Nørgaard[a,b], Martin Margold[c], John D. Jansen[d], Izabela Szuman[c,e], Mariya Lukyanycheva[f], Jane Lund Andersen[a], Vivi Kathrine Pedersen[a], Jesper Olsen[g], Lee B. Corbett[h], Paul R. Bierman[h] and Mads Faurschou Knudsen[a]

[a]Department of Geoscience, Aarhus University, Aarhus, Denmark; [b]Near Surface Land and Marine Geology, Geological Survey of Denmark and Greenland, Aarhus, Denmark; [c]Department of Physical Geography and Geoecology, Charles University, Prague, Czechia; [d]GFÚ Institute of Geophysics, Czech Academy of Sciences, Prague, Czechia; [e]Institute of Geoinformation and Geoecology, Adam Mickiewicz University, Poznań, Poland; [f]Institute of Archaeology and Anthropology, Azerbaijan National Academy of Sciences, Baku, Azerbaijan; [g]Department of Physics and Astronomy, Aarhus University, Aarhus, Denmark and [h]Rubenstein School for Environment and Natural Resources, University of Vermont, Burlington, VT, USA

Abstract

The glacial history of northeast Siberia is poorly understood compared with other high-latitude regions. Using ^{10}Be and ^{26}Al exposure dating together with remote sensing, we have investigated the glacial history of a remote, formerly glaciated valley in the Tas-Kystabyt Range of the Chersky Mountains in central northeast Siberia. Based on measurements from moraine boulders and bedrock samples, we find evidence for deglaciation of the valley 45.6 ± 3.4 ka ago, that is during the peak of Marine Isotope Stage 3. Satellite imagery of the range reveals at least two generations of moraines in other nearby valleys, indicating that multiple stages of glaciation took place across the Tas-Kystabyt Range. Based on calculated equilibrium-line altitudes, we speculate that the outer set of moraines is linked to the 45.6 ± 3.4 ka deglaciation event identified by our dating, while the inner generation of moraines is associated with a younger glaciation event, possibly the last glacial maximum (LGM). Thus, our results reaffirm current impressions that the maximum ice extent during the last glacial cycle was reached before the global LGM in northeast Siberia.

Keywords: Mountain glaciers; Glacial moraines; Exposure dating; Cosmogenic nuclides

Introduction

Northeast Siberia is characterized by some of the most extreme continental climate found in the Northern Hemisphere. The glacial history of high northern latitudes generally follows the global climate trends recorded in the benthic marine δ^{18}O record (Lisiecki and Raymo, 2005; Stokes et al., 2012; Simms et al., 2019). However, interior continental settings often display anomalies in this regard, with local glacial expansion asynchronous with global ice-volume trends (Svendsen et al., 2004; Ward et al., 2007; Batchelor et al., 2019), so it is possible that the cold, landlocked climate of northeast Siberia creates an environment in which glaciation may not follow global patterns. While most Northern Hemisphere ice masses reached their overall maximum extent over the last glacial cycle during the last glacial maximum (LGM) 26–19 ka ago (Svendsen et al., 2004; Barr and Clark, 2012a; Batchelor et al., 2019; Simms et al., 2019; Dalton et al., 2022a, Halsted et al., 2024), glaciers in northeast Siberia may have reached their maximum well before the global LGM.

Corresponding author : Jesper Nørgaard; Email: jesn@geus.dk

Cite this article: Nørgaard J. *et al*., 2025. A late Pleistocene glacial maximum during MIS 3 in the Chersky Mountains, central northeast Siberia. *Quaternary Research*, 1–11. https://doi.org/10.1017/qua.2025.20

The general consensus is that LGM ice formation in northeast Siberia was limited to alpine-style glaciers and mountain ice fields (Gualtieri et al., 2000; Glushkova, 2001; Brigham-Grette et al., 2003; Nørgaard et al., 2023), with some regions, such as the Verkhoyansk Mountains (Fig. 1), remaining more or less ice free during the LGM (Stauch and Gualtieri, 2008; Zech et al., 2011; Barr and Clark, 2012a). While the maximum ice extent during the last glacial cycle in northeast Siberia is reported to have occurred early (pre-global LGM), an exact timing has not been established for the whole region and may possibly have varied within it (Gualtieri et al., 2000; Brigham-Grette et al., 2003; Nørgaard et al., 2023) due to orographic and climatic variations across the vast mountainous region (Glushkova, 2001). The glacial history could have been controlled by many local factors such as the region's cold, continental climate, complex topography, and/or the frigid, periodically ice-covered Arctic Ocean to the north influencing moisture availability. However, previous work has also speculated that the limited extent of glaciation at the time of the global LGM is primarily a result of reduction in moisture supply connected to the growth of the western part of the Eurasian Ice Sheet blocking circulation of the westerlies (Krinner et al., 2011; Zech et al., 2011; Barr and Clark, 2012a). Going further back in time, several studies have shown that the ice extent in northeast Siberia during Marine Isotope Stage (MIS) 6 surpassed any of the glaciations

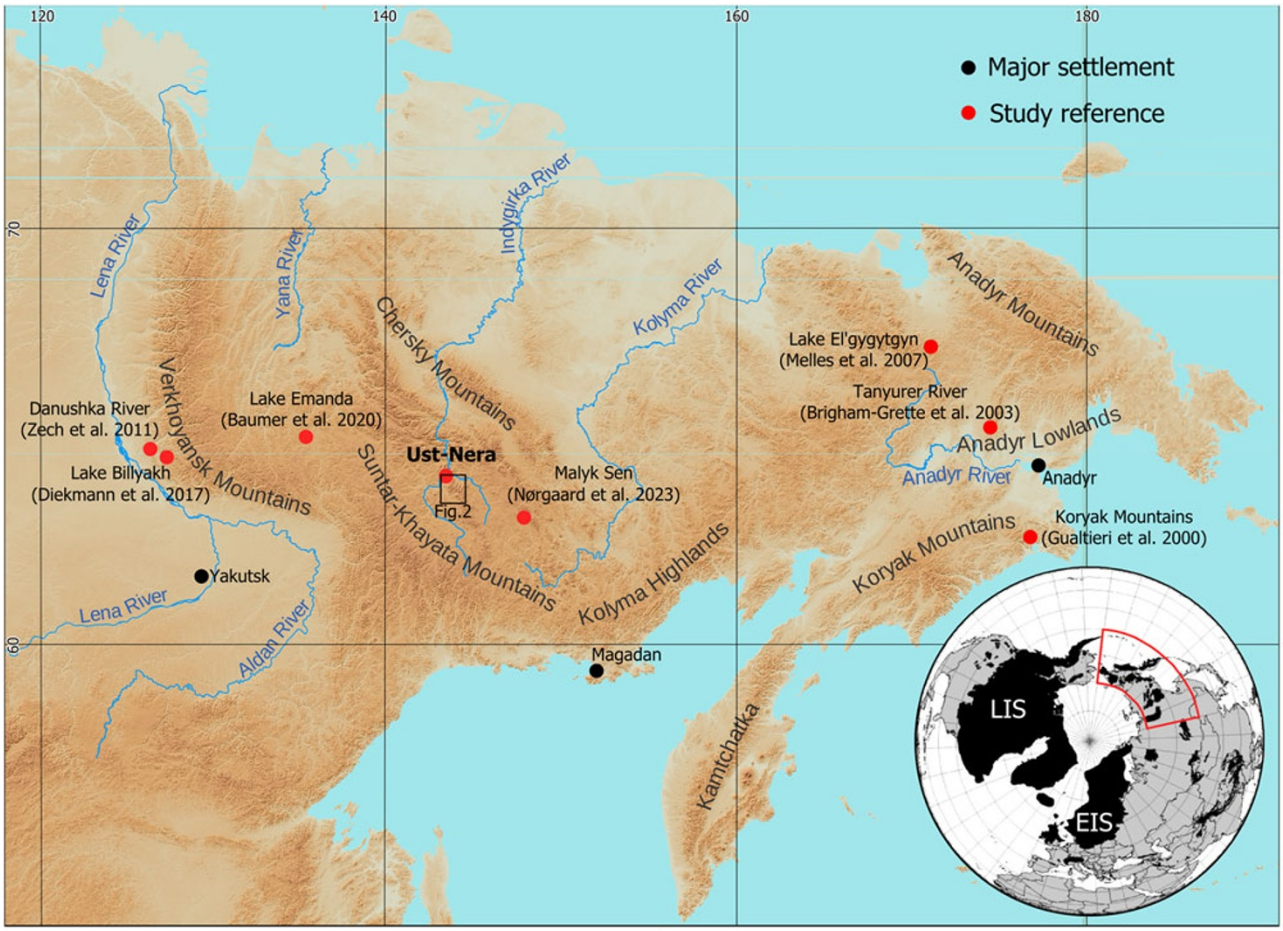

Figure 1. Overview map of the northeast Siberian region. Localities from studies mentioned in the text are marked with red dots (Gualtieri et al., 2000; Brigham-Grette et al., 2003; Melles et al., 2007; Stauch and Gualtieri, 2008; Zech et al., 2011; Diekmann et al., 2017; Baumer et al., 2020; Nørgaard et al., 2023). Major mountain chains, rivers, and settlements are also labeled. The bottom right insert is adapted from Ehlers and Gibbard (2007) and shows the Northern Hemisphere ice extent at the LGM, including the Laurentide Ice Sheet (LIS) and the Eurasian Ice Sheet (EIS). The digital elevation map is based on "General Bathymetric Chart of the Oceans" (https://gebco.net).

that occurred during the last glacial cycle (Stauch et al., 2007; Nørgaard et al., 2023). Moraines of the penultimate glacial maximum remain the oldest dated landforms in northeast Siberia so far, but studies have reported geomorphological evidence of undated glacial landforms that could belong to older, even more extensive glaciations (Brigham-Grette et al., 2003; Stauch and Gualtieri, 2008; Nørgaard et al., 2023), such as the mid-Pleistocene superglaciations tentatively associated with MIS 16 or 12 (Batchelor et al., 2019).

It remains difficult to ascertain clear spatial and temporal patterns in the glacial history of northeast Siberia with only a handful of chronological studies to rely on in an extensive mountain landscape spanning over 1 million km^2 of formerly glaciated terrain (Barr and Clark, 2012b). Thus, a more extensive coverage of age constraints is needed to improve our understanding of spatial variations in this region's complex glacial history. Specifically, the vast mountainous landscape at the heart of the region, which includes the Chersky Range and the Suntar-Khayata Mountains, remains understudied and represents a large knowledge gap between the eastern and western parts of the region (Fig. 1). Here, we present cosmogenic exposure age results from a valley in the Tas-Kystabyt Range of the Chersky Mountains close to the settlement of Ust-Nera and far from any existing studies of glacial chronology, revealing a so-far undocumented deglaciation around 46 ka ago in the area.

Study area and fieldwork

The Yuryuyete River valley

In the field, we investigated the U-shaped valley of the Ambar-Yuryuyete (Амбар-Юрюете) River that lies within the Tas-Kystabyt Range of the Chersky Mountains. It is hereafter referred to simply as the Ambar-Yuryuyete Valley. It is located at approximately 64.5°N, 143.3°E by the confluence of the large Indigirka River and the smaller Nera River (Fig. 1). The present climate of the nearby settlement Ust-Nera (Fig. 2A), located approximately 6 km away and 500 m lower than the sampling site, is mild during summer, with daily temperatures averaging ~12°C. Winters are very cold and dry, with mean temperatures in January as low as −44°C (https://www.timeanddate.com/weather/russia/ust-nera/climate, accessed 25 March 2024). Subzero temperatures persist from mid-September to early May. Precipitation outside the main summer period (mid-May to mid-September) is low and totals ~50 mm/yr based on weather reports from 2005 to 2015 (Sakha, Russia, 64.57°N, 143.24°E, 492 m above sea level [m asl]) making for a light snow cover (<1 m) typically lasting until early June. The surrounding mountains reach elevations up to 2000 m, while the elevation of the valley floor and the top of the valley headwall are approximately 650 and 1400 m asl, respectively. The valley faces north, with the ridges on both sides of the valley striking north-south. The elevation gain from the bottom of the valley to the tor-studded ridge

https://doi.org/10.1017/qua.2025.20 Published online by Cambridge University Press

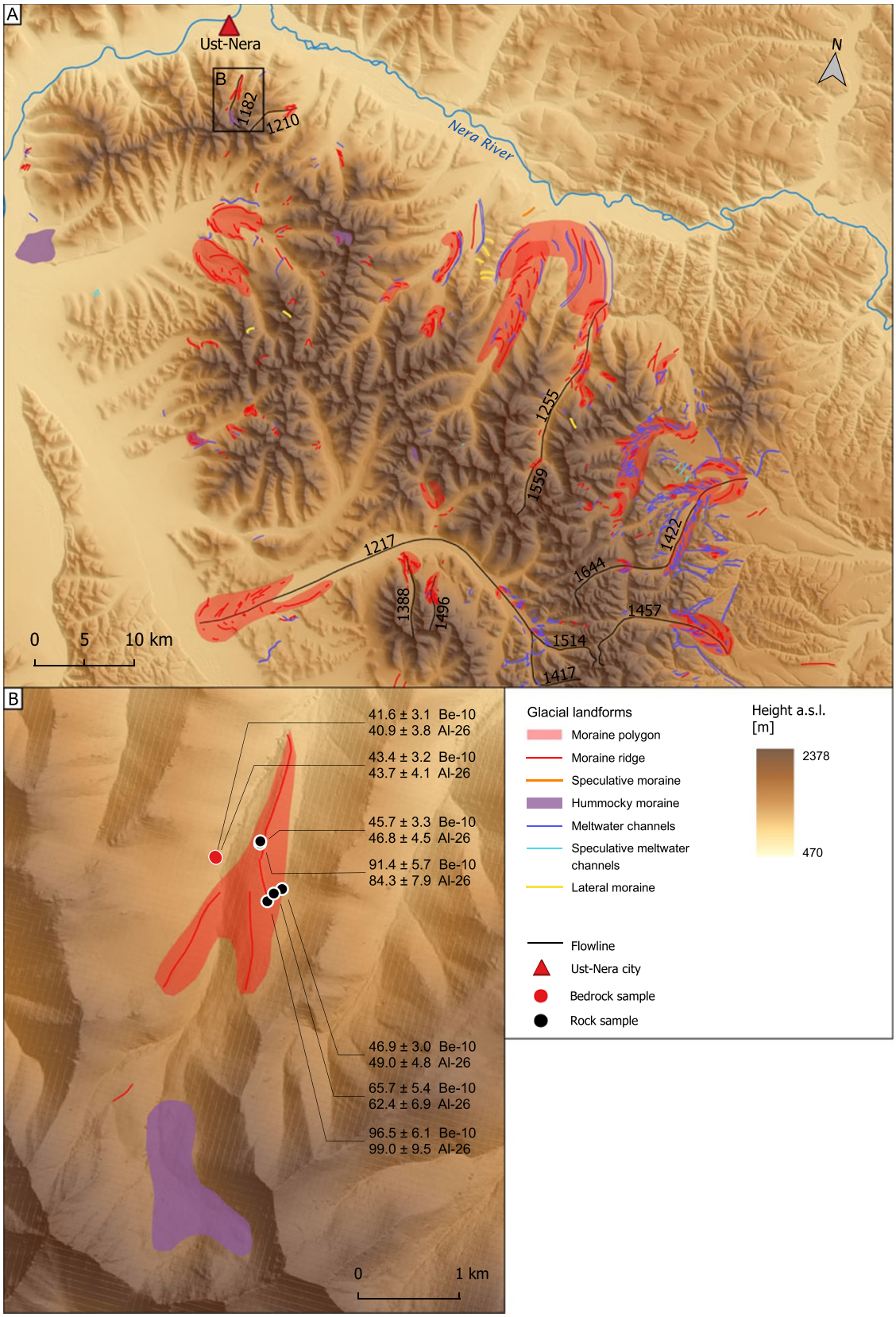

Figure 2. (A) Overview map of geomorphological features in the Tas-Kystabyt Range. Black lines mark the valley distances from toe to headwall and numbers in black are the corresponding equilibrium line altitude (ELA) estimates. (B) Close-up of the geomorphology of the valley at Ust-Nera. Black dots show the locations of the sampled boulders, red dot shows the location of the sampled bedrock. Numbers indicate exposure ages (in ka). The elevation model is ArcticDEM (Porter et al., 2018).

https://doi.org/10.1017/qua.2025.20 Published online by Cambridge University Press

crests is approximately 200 m. The valley is sparsely covered in coniferous trees, bushes, and scrub, with thinning vegetation cover toward the upper reaches of the valley. Within the valley is a lateral end moraine and a well-developed cirque with steep headwalls in the uppermost part of the valley (Fig. 2B).

Field conditions and sample collection

Fieldwork in the Tas-Kystabyt Range in August 2021 was limited to the Ambar-Yuryuyete Valley due to logistical reasons. We traversed the Ambar-Yuryuyete Valley on foot in search of boulders and bedrock outcrops suitable for exposure dating. Most of the terrain was overgrown with vegetation, and the moraine was not easily distinguishable in the field, except for scattered moraine boulders up to a few meters in height. The boulders and bedrock exposed in the valley, as well as the tors on the ridge crests, all had a granitic composition, suggesting that the boulders were derived from local bedrock. In total, we collected seven samples: (1) five samples from boulders on the moraine in the valley center and (2) two samples from bedrock outcrops on the western side of the valley ~10 m above the valley base where the Ambar-Yuryuyete River runs.

Methods

Geomorphological mapping and snow-line approximation

We mapped the glacial geomorphology of the Tas-Kystabyt Range using hill-shaded imagery derived from the ArcticDEM v. 3 mosaic with 2 m spatial resolution (Porter et al., 2018) in the QGIS Geographic Information System (Fig. 2). Moraines were the principal landform of interest. Other mapped landforms include meltwater channels and hummocky terrain. Landforms that were identified with some uncertainty were included in the mapping category "speculative" (moraines or meltwater channels). For approximation of the equilibrium line altitude (ELA), we used toe-to-headwall altitude ratios (Benn and Lemkuhl, 2000) of 0.4 and assumed the ice-surface altitude to be 50 m below the headwall crests. Both altitudes were derived from the ArcticDEM maps once the features had been mapped.

Cosmogenic nuclide measurements

Samples were collected for cosmogenic nuclide exposure dating using an angle grinder, hammer, and chisel, targeting the uppermost 2–3 cm of the rock surface. Quartz separation was conducted at the Aarhus University Cosmogenic Nuclide Laboratory, following standard procedures (Kohl and Nishiizumi, 1992). We verified quartz purity by inductively coupled plasma optical emission spectrometry (ICP-OES) and performed additional acid etching on a subset of the samples as needed to reduce the concentration of cations, including Al, Ca, Fe, K, Mg, Na, and Ti.

We extracted beryllium (n = 7) and aluminum (n = 7) from the samples in the NSF/UVM Community Cosmogenic Facility using methods described in Corbett et al. (2016) and 20.64–21.47 g of quartz per sample. The batch included two full processing blanks and a reference material aliquot (UVM-A; Corbett et al., 2024). We spiked the samples with ~250 µg of ^{9}Be using a carrier termed UVM-SPEX, created from a dilution of SPEX 10,000 ppm Be standard, with a resulting Be concentration of 304 µg/mL (Supplementary Table S1). We spiked samples with Al as needed to ensure at least 1500 µg of total Al, based on the native Al contained in the quartz, using a SPEX commercial Al standard with a concentration of 1000 ppm.

We quantified total Al in the samples (Supplementary Table S2) by ICP-OES immediately following sample digestion. Following standard procedures (Corbett et al., 2016), we removed replicate aliquots from the samples by mass (representing ~2% and ~4% of the sample, respectively), added 25 µL H_2SO_4 to each, evaporated the HF, then diluted the residual H_2SO_4 droplets by mass with a 0.25% H_2SO_4 solution containing 10 ppm of yttrium to serve as an internal standard.

Accelerator mass spectrometry analysis (AMS) was performed at the Aarhus AMS Centre, Department of Physics and Astronomy, Aarhus University. For ^{10}Be/^{9}Be, measured ratios were normalized to primary standard ICN-01-5-4 with a ^{10}Be/Be ratio of 2.85×10^{-12} (Nishiizumi et al., 2007). For ^{26}Al/^{27}Al, analyses were normalized to primary standard ICN-01-5-2 with a ^{26}Al/Al ratio of 1.82×10^{-12} (Nishiizumi, 2004). We corrected samples for backgrounds using the average and standard deviation of blanks associated with the samples $(4.65 \pm 1.26) \times 10^{-15}$ for ^{10}Be/^{9}Be and $(2.05 \pm 4.64) \times 10^{-15}$ for ^{26}Al/^{27}Al derived from a single blank (Supplementary Table S3). We propagated the blank uncertainties in quadrature. For ^{10}Be/^{9}Be, background-corrected sample ratios range from 5.96×10^{-13} to 1.40×10^{-12}, with the blank correction representing 0.3–0.8% of the sample ratios. For ^{26}Al/^{27}Al, background-corrected sample ratios range from 5.53×10^{-13} to 1.39×10^{-12}, with the blank correction representing 0.1–0.4% of the sample ratios.

Exposure ages and outlier detection were calculated using the online calculators formerly known as the CRONUS-Earth online calculators (Balco et al., 2008), applying the LSDn time-dependent scaling scheme of Lifton et al. (2014) and global production calibration (Borchers et al., 2016). In these calculations, we have assumed a sample density of 2.65 g/cm^3 typical of granitic rocks. Topographic shielding and snow shielding are calculated following the methods outlined in Gosse and Phillips (2001).

Results

Remote sensing of glacial landforms

Geomorphological mapping based on satellite imagery (ArcticDEM v. 3) reveals sizable (kilometer-scale) moraines in most main valleys draining the Tas-Kystabyt Range (Fig. 2A). One to two terminal or recessional moraines typically occur upvalley from the terminal moraines associated with the most extensive glaciations. The mapped moraines indicate past glaciation that took the form of an extensive mountain ice field southeast of the Ambar-Yuryuyete Valley, possibly during several distinct periods, with the main outlet glaciers reaching several tens of kilometers from the ice divide to the ice front.

In contrast, the northwestern parts of the range, where the Ambar-Yuryuyete Valley is located, contain little evidence of former glaciation besides isolated and solitary moraines in a few of the valleys (Fig. 2A). In most of the other short, steep-sloping valleys that constitute this part of the range, we did not map any moraines. The Ambar-Yuryuyete Valley, where we collected samples, stands out as one of the few valleys with a moraine in this northernmost part of the Tas-Kystabyt Range. The valley moraine is a 2.5-km-long slope-parallel lateral moraine that transitions into a narrow terminal moraine downstream (250-m-long segment oblique to the

https://doi.org/10.1017/qua.2025.20 Published online by Cambridge University Press

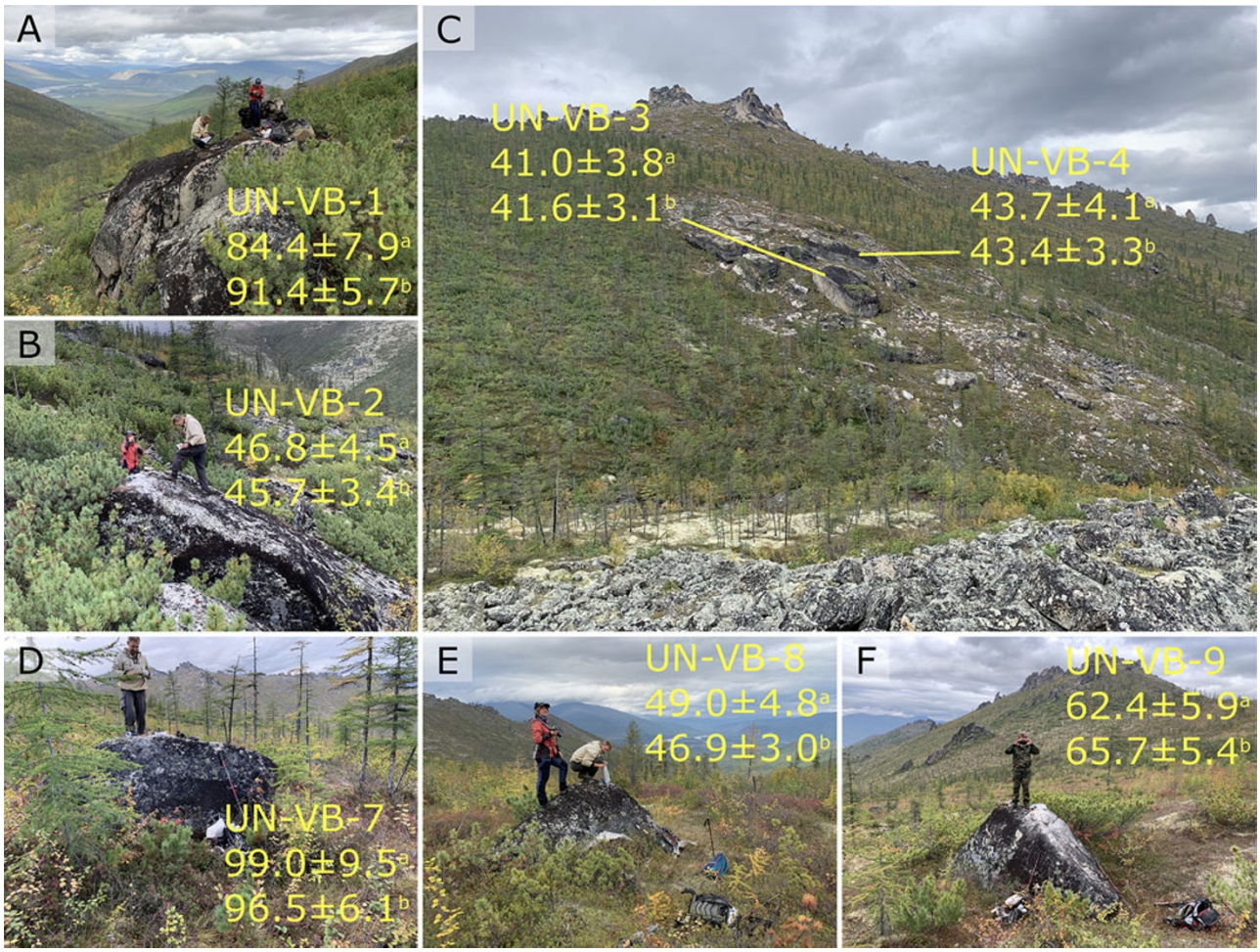

Figure 3. (A-F) Photos of sampled boulders and bedrock. Superscript a and b denote apparent exposure ages of ^{26}Al and ^{10}Be respectively, which are corrected for topographic shielding but not potential snow shielding.

thalweg), tracing the snout of the former valley glacier (Fig. 2B). Further upvalley, an area of hummocky ground occurs at the foot of the cirque headwall that might relate to the former presence of a small cirque glacier or, alternatively, represents a small rock glacier generated from debris falling off the steep headwall. Consequently, there is no clear geomorphological evidence for more limited glacial advances younger than the solitary moraine we sampled, nor is there evidence for larger glaciations lower down the Ambar-Yuryuyete Valley in either the valley itself or in the Indigirka and Nera valleys beyond the small-valley mouth (Fig. 2A). Shapefiles of all mapped features can be found in the Supplementary Material (filename: Supp.Fig.2_shp).

Reconstruction of paleo-ELAs (12 in total) was carried out where both the toe and headwall could be reliably identified in the valleys and yielded an ELA of 1182 m asl for the Ambar-Yuryuyete Valley and 1210 m asl for the neighboring valley on the east side. In the valleys to the southwest of the range, the many identified moraines are associated with different ELAs that range from 1217 m asl to 1644 m asl. The ELA for the maximum glacial extent in the largest west-draining valley is 1217 m asl, but other mapped moraines farther up the valley yield ELAs of 1417 m asl 33 km upvalley and 1514 m asl 39 km upvalley, respectively. The average ELA for the minimum glacial extent in the western part is 1466 m asl.

Ambar-Yuryuyete Valley exposure ages

Calculated ^{10}Be exposure ages corrected only for topographic shielding range from 41.6 ± 3.1 to 96.5 ± 6.1 ka, while calculated ^{26}Al ages range from 41.0 ± 3.8 to 99.0 ± 9.5 ka, with the two bedrock samples UN-VB-3 and UN-VB-4 providing the youngest ages (Fig. 3C, Table 1). The five boulder samples show considerable variation in calculated ages, with ^{10}Be ages ranging from 45.7 ± 3.4 to 96.5 ± 6.1 ka and ^{26}Al ages ranging from 46.8 ± 4.5 to 99.0 ± 9.5 ka. The boulder ages do not indicate any immediate correlation between sampling location and sample ages (Fig. 2B). For all samples, the ^{10}Be and ^{26}Al ages overlap within 1σ uncertainty regardless of sample type and location. Because the bedrock samples were at the ground surface level, it is more likely that they were continuously covered by the annual snow cover of roughly 50 cm (based on the ~50 mm/yr winter precipitation) compared with the moraine boulders that each stood >1.5 m above ground (Fig. 3, Table 1). The boulders possibly experienced significantly less snow cover due to the wind remobilizing the freshly fallen snow. Accounting for snow shielding (see Supplementary Material) of the bedrock samples UN-VB-3 and UN-VB-4 yields calculated ^{10}Be ages of 43.3 and 45.2 ka and ^{26}Al ages of 42.7 and 45.6 ka for these two samples, respectively (Table 1).

https://doi.org/10.1017/qua.2025.20 Published online by Cambridge University Press

Table 1. Cosmogenic nuclide data. Coordinates and elevations are measured using handheld GPS and cross-checked against the ArcticDEM elevation model (Porter et al., 2018).[a]

Name	Lat. (°N)	Long. (°E)	Elev. (m asl)	Type	Sample thickness (cm)	Boulder dimensions[b] (width × width × height) (m)	Topographic shielding	Nuclide	Concentration (10^3 at/g)	Uncertainty (10^3 at/g)	Age (ka)	Int. 1-σ (ka)	Ext. 1-σ (ka)	50 cm snow corr. age (ka)	Ext. 1-σ (ka)
UN-VB−1	64.51454	143.27109	1081	Boulder	2.25	5 × 5 × 5	0.9862	Be−10	1081	17	91.4	1.5	5.7	—	—
								Al−26	6931	169	84.4	2.1	7.9	—	—
UN-VB−2	64.51454	143.27109	1081	Boulder	2	8 × 4 × 3	0.9906	Be−10	550	23	45.7	1.9	3.4	—	—
								Al−26	3938	149	46.8	1.8	4.5	—	—
UN-VB−3	64.51295	143.26236	998	Bedrock	2.5	—	0.9878	Be−10	462	21	41.6	1.9	3.1	43.3	3.3
								Al−26	3190	98	41.0	1.3	3.8	42.7	4.0
UN-VB−4	64.51295	143.26236	998	Bedrock	4.5	—	0.9880	Be−10	474	21	43.4	2.0	3.3	45.2	3.4
								Al−26	3347	108	43.7	1.4	4.1	45.6	4.3
UN-VB−7	64.50961	143.27390	1050	Boulder	1.5	3 × 2 × 1.5*	0.9948	Be−10	1125	21	96.5	1.9	6.1	—	—
								Al−26	7976	245	99.0	3.2	9.5	—	—
UN-VB−8	64.51082	143.2758	1081	Boulder	3	2 × 2 × 2*	0.9940	Be−10	562	13	46.9	1.1	3.0	—	—
								Al−26	4103	172	49.0	2.1	4.8	—	—
UN-VB−9	64.51035	143.27502	1095	Boulder	3	4 × 3 × 2*	0.9955	Be−10	794	45	65.7	2.0	5.4	—	—
								Al−26	5260	163	62.4	3.8	5.9	—	—

[a]All uncertainties are reported as 1σ external errors.
[b]Boulder height was estimated as the distance from the ground to the highest point on the boulder.
An asterisk (*) denotes boulder height above terrain as opposed to full height estimate.

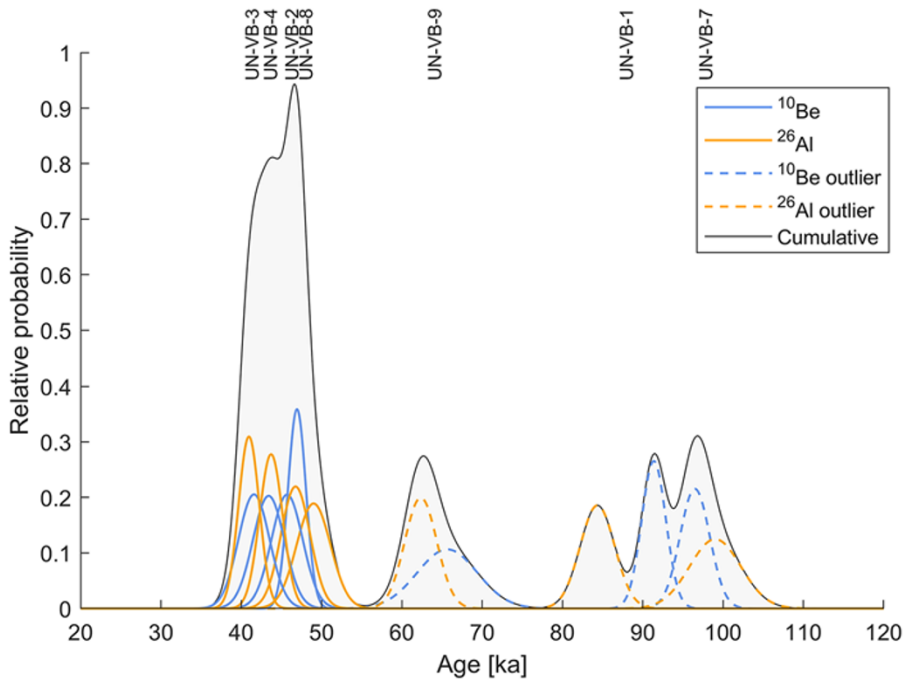

Figure 4. Gaussian distributions of the calculated exposure ages with internal errors as standard deviation. UN-VB-3 and UN-VB-4 ages are corrected for 50 cm snow shielding to help illustrate the clustering. Detected outliers have been indicated with dashed lines. The black line is the cumulative age distribution.

Discussion

Calculated exposure ages and inherited nuclides

The agreement between the ^{10}Be and ^{26}Al ages suggests that all samples experienced relatively simple exposure histories, which in this context means one or few periods of exposure within recent times and insufficient shielding of the samples to produce significant decay of either nuclides. However, we observe a scatter in the exposure ages among the five boulder samples. Scatter in exposure ages is typically explained by either (1) inheritance of nuclides accumulated in the rocks before moraine formation, rendering the apparent ages of some of the boulder samples too old (Fabel and Harbor, 1999; Applegate et al., 2010; Heyman et al., 2011); or (2) postglacial shielding or erosion, which could render some of the exposure ages too young (Fabel and Harbor, 1999; Applegate et al., 2010; Heyman et al., 2011). Here, we favor the first option for the following reasons: (1) the skewness of the age distribution, including multiple young samples with overlapping uncertainties and a tail of older ages (Fig. 4); and (2) outlier detection analysis on the sample set suggests the three oldest samples are outliers. Outlier detection was done using the CRONUS-Earth online calculator, which performs a χ^2-based pruning of the data (Bevington and Robinson, 1992). Hence, the three boulders that likely contain inherited nuclides are UN-VB-1, UN-VB-7, and UN-VB-9, based on their ^{10}Be exposure ages (91.4 ± 5.7, 96.5 ± 6.1, and 65.7 ± 5.4 ka) and ^{26}Al exposure ages (84.4 ± 7.9, 99.0 ± 9.5, and 62.3 ± 5.9 ka), respectively. These three boulders were likely picked up by an advancing ice and emplaced at their current location in such a way that the upward-facing surface we sampled contained a significant concentration of nuclides produced during previous periods of surface exposure. It is not possible to determine whether the inherited concentrations relate to orientation and rock-depth during previous exposure or the duration of that exposure.

In contrast, the two remaining boulders were likely emplaced in such a way that the sampled surfaces contained an insignificant concentration of inherited nuclides from prior exposure. This could be either because these boulders were sourced from considerable depth (requiring deep erosion) or because they were emplaced upside down compared with their previous orientation before glacial transport. The two bedrock samples were found in the low-central part of the valley, where glacial erosion and scouring would have been most efficient, implying that the nuclide inventories of these bedrock samples likely would have been reset during the last glacial event. The fact that two boulders yield ^{10}Be and ^{26}Al ages that confidently overlap the ^{10}Be and ^{26}Al bedrock ages suggests that these four samples belong to the same population and that their nuclide inventories reflect a simple exposure history that constrains the last deglaciation event of the Ambar-Yuryuyete Valley. This presents the simplest scenario that accounts for the nuclide inventories in both bedrock and boulder samples. In any other conceivable scenario, it is unlikely that the ages derived from the two youngest boulder samples would overlap the ages associated with the bedrock samples.

Nevertheless, given the relative spread among the apparent exposure ages, we cannot completely rule out the possibility that deglaciation occurred before MIS 3, perhaps even as early as MIS 6. It is possible that some or all samples were covered by sediments for extensive periods of time after deglaciation, resulting in incomplete exposure after the last deglaciation event. It has been shown in earlier publications that postdepositional shielding is often the most important source of scatter among exposure ages of glacial boulders and that the maximum apparent exposure age should be viewed as a minimum deglaciation age for boulder groups with a wide age scatter (Heyman et al., 2011). However, we do not think that this is the case for the Ambar-Yuryuyete Valley samples. First, a group of three closely spaced boulders (UN-VB-7, UN-VB-8, and UN-VB-9) of similar height (~2 m) yield widely different apparent ^{10}Be ages (96.5 ± 6.1, 46.9 ± 3.0, and 65.7 ± 5.4 ka), while two other boulders (UN-VB-1 and UN-VB-2) located some ~500 m away also yield different ^{10}Be ages (91.4 ± 5.7, and 45.7 ± 3.4 ka). Second, the younger ages in both groups of boulders are consistent

https://doi.org/10.1017/qua.2025.20 Published online by Cambridge University Press

with the ages of bedrock samples collected next to the moraine. It is difficult to explain this age pattern with postdepositional shielding, as the shielding would have to vary locally among closely spaced boulders. It is, on the other hand, easier to reason that the apparent exposure age shared by the two bedrock samples and the two youngest boulders reflects a deglaciation event at 45.6 ± 3.4 ka and that the three remaining boulders contain an inherited nuclide inventory. The large inherited nuclide inventory observed in two of the samples (UN-VB-1 and UN-VB-7) likely reflects the cold and exceptionally dry climate in the region, implying that erosion may have been limited because the glaciers were frozen to the ground during large parts of the time. Such patterns have also been observed in boulder and bedrock samples from areas in Greenland occupied by cold-based glaciers (e.g., Søndergaard et al., 2020).

Deglaciation timing of the Tas-Kystabyt Range

Disregarding the samples affected by inheritance, we calculate a weighted mean age of 45.6 ± 3.4 ka using both ^{10}Be and ^{26}Al from the two bedrock samples with snow shielding (UN-VB-3 and UN-VB-4) and the two youngest boulders without snow shielding (UN-VB-2 and UN-VB-8). We consider this mean exposure age to be the best possible estimate for the most recent deglaciation of the valley. However, given the low elevation of the weather station (∼500 m asl) relative to the site (998–1095 m asl), the 50 cm snow cover might be seen as a minimum. Excess snow above the 50 cm already considered would push the age estimate toward older ages. As an example, adding another 1 m of snow cover during the nine winter months to all four samples considered yields a calculated mean of 48.6 ± 4.0 ka. Which is still in agreement with our initial estimate within uncertainty. Consequently, we arrive at a deglaciation age for this region that in any case corresponds to the global MIS 3.

Relating the deglaciation age to our regional geomorphological mapping, we suggest that the 45.6 ± 3.4 ka deglaciation event is linked to the outer of the two generations of moraines we were able to identify in several valleys in the southeastern parts of the Tas-Kystabyt Range using remote sensing (Fig. 2). This suggestion is based mainly on two weak clusters of the ELAs one around ∼1200 m and another around ∼1500 m. Given the relatively small extent of the Tas-Kystabyt Range, we find it reasonable to assume synchronous growth and retreat of ice masses across the range. Thus, we suggest that the lower ELAs could be associated with the deglaciation event at 45.6 ± 3.4 ka, and the higher ELAs linked to a younger, smaller deglaciation event that possibly could represent ice retreat after the LGM, although we acknowledge that these end-moraine features typically are indicative of equilibrium positions, while the exposure ages are indicative of ice retreat.

Regional comparison and lack of LGM glaciation

Geomorphological mapping did not reveal any other glacial landscape features in the Ambar-Yuryuyete Valley that could represent significant additional ice advances, either above or below the sampled moraine, other than an area of hummocky terrain immediately below the valley headwall, possibly indicating the existence of a small cirque glacier. The lack of geomorphological evidence for other advances, the preservation of the moraine in this valley, and our deglaciation age of 45.6 ± 3.4 ka thus largely rule out the possibility of an LGM ice advance occurring inside this valley, because even a cold-based, nonerosive reglaciation could be expected to leave behind a moraine from the debris falling off the steep slopes above the glacier and transported to the glacier's snout. Additionally, this is also supported by our calculated ages showing no indication of prolonged shielding. If an LGM glaciation did occur in the Tas-Kystabyt Range, we suggest that it did not reach the Ambar-Yuryuyete Valley and only covered the southeastern part of the range (Fig. 2). Alternatively, the LGM could have produced the aforementioned small cirque glacier, which would have been a solitary feature at the time.

An absence of evidence for LGM glaciation in the Ambar-Yuryuyete Valley is at odds with global trends but aligns with the current interpretation of the glacial history of the Verkhoyansk Mountains (Fig. 1), where previous work suggests that glaciers were largely absent during the LGM (Stauch and Lehmkuhl, 2010). The latest moraine deposit in the Verkhoyansk Mountains slightly predates the moraine age in the Ambar-Yuryuyete Valley at around 50 ka following optically stimulated luminescence (OSL) dating by Stauch and Lehmkuhl (2010); however, this is largely similar to our deglaciation timing within error. Comparable findings have also been reported elsewhere in northeast Siberia (Fig. 5). Notably, Gualtieri et al. (2000) concluded from ^{36}Cl measurements on bedrock in the Anadyr Lowlands that the area has been ice free since ∼53 ka, while Brigham-Grette et al. (2003) dated several erratics in the age range 36 to 69 ka using ^{36}Cl in the Tanyurer River valley, even if the lack of consistency between these ages obscured any more precise age estimate. In Kamchatka, Bäumler and Zech (2000) reported deglaciation concluded before 40 ka, as indicated by a dated tephra overlying glacial till.

At all these locations, various other glacial features identified higher up in the mountains were interpreted to indicate a very limited ice extent during the LGM. At Lake Malyk, the study site closest to the Ambar-Yuryuyete Valley, an intermediate moraine ridge, sandwiched between an LGM and an MIS 6 moraine, has been dated with cosmogenic ^{10}Be to MIS 4 or MIS 5, but the possibility that this middle moraine was deposited during MIS 3 cannot be excluded (Nørgaard et al., 2023). Two sediment cores from Lake Billyakh and Lake Emanda of the Verkhoyansk Mountains do not reach as far back as MIS 4, but both cores terminate in what could be glacial deposits toward the end of MIS 4 or the onset of MIS 3 (Diekmann et al., 2017; Baumer et al., 2020). We caution, though, that these two timings (51 ka and 57 ka) are based on radiocarbon ages very close to the limits of the method; hence, they could very well represent minimum ages.

It is possible that many of the abovementioned observations reflect the same glaciation period of northeast Siberia, with variable timings potentially being explained by the different dating methods applied (and their inherent uncertainties) as well as variations in local climatic and orographic conditions. On the other hand, the single 2.5 km lateral end moraine occupying the Ambar-Yuryuyete Valley is not a typical feature compared with the rest of the Tas-Kystabyt Range, leaving it unclear whether our own age represents a local oddity.

Global evidence of MIS 3 glaciations

A maximum ice extent within the last glacial cycle during MIS 3, as indicated by our results, is uncommon in a global context (Batchelor et al., 2019; Dalton et al., 2022b). Evidence of significant ice retreat during MIS 3 remains scarce, partly because most evidence would have been destroyed by the subsequent LGM ice advance. However, ice advances and retreats have been associated with MIS 3 in several other studies and areas (Hughes et al., 2013), including western Finnish Lapland (Salonen et al.,

https://doi.org/10.1017/qua.2025.20 Published online by Cambridge University Press

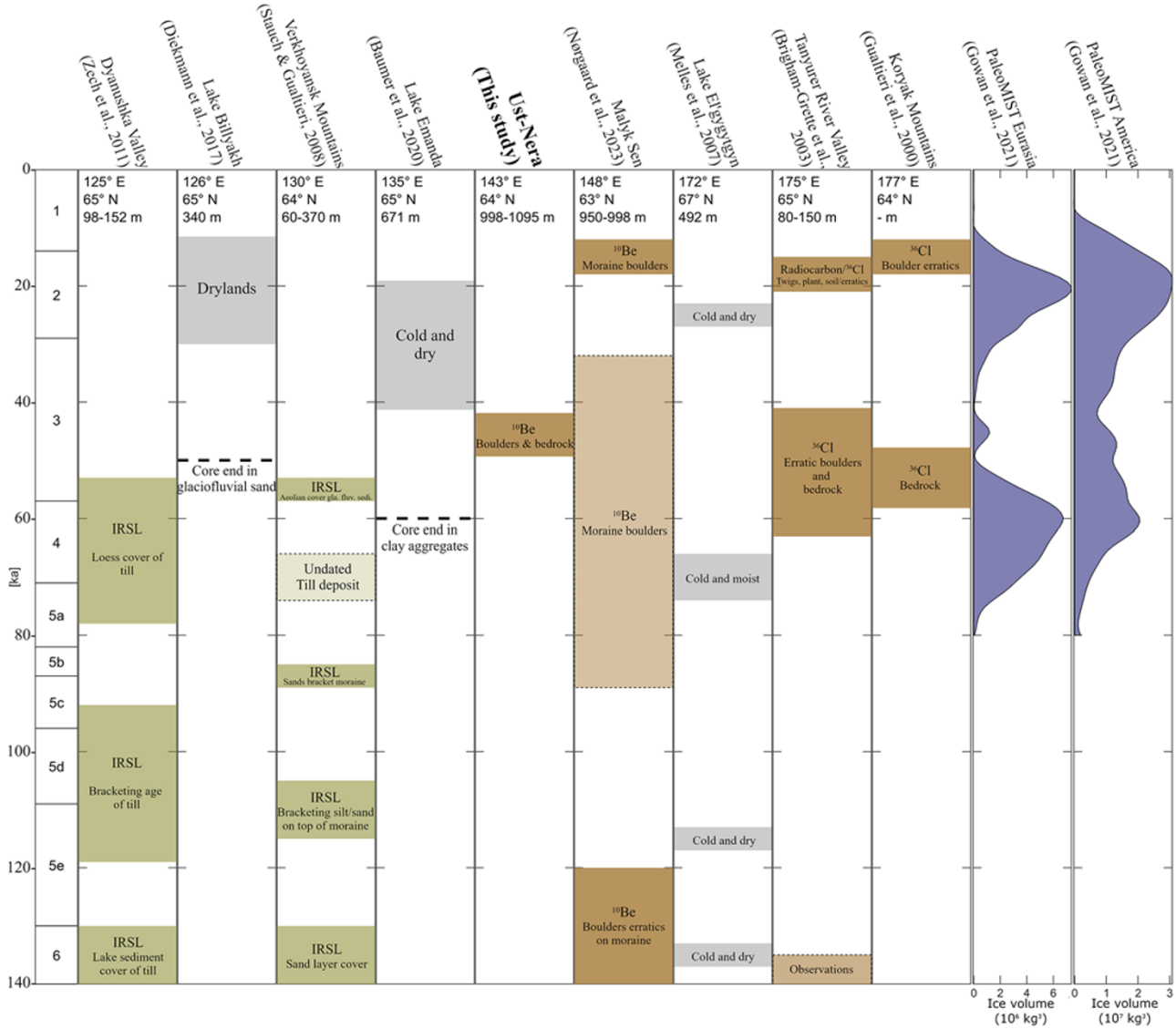

Figure 5. A compilation of chronological studies of glacial features in northeast Siberia sorted from west to east (left to right: Gualtieri et al., 2000; Brigham-Grette et al., 2003; Melles et al., 2007; Stauch and Gualtieri, 2008; Zech et al., 2011; Diekmann et al., 2017; Baumer et al., 2020; Gowan et al., 2021); Nørgaard et al., 2023). Boxes indicate observations. Brown colors are exposure dates, which are typically indicative of glacial retreat; heights of the boxes indicate uncertainty on measurements/spreads of ages at the site. Green colors are infrared-stimulated luminescence (IRSL) bracketing ages of moraines; heights of the boxes indicate upper and lower limits for the moraine age. Dashed outlines and paler colors indicate greater than analytical uncertainty with regard to timing, that is, lack of numerical constraint or ambiguous ages. Gray colors are climatic conditions; heights of the boxes indicate duration. The last two panels show the estimated ice volumes of the Eurasian and North American ice sheets during the last 80 ka (Gowan et al., 2021).

2014), the west coast of Norway (Mangerud et al., 2011), the Yukon Territory (Ward et al., 2007), the Davis Strait (Seidenkrantz et al., 2019), two advances of the Laurentide Ice Sheet into the Upper Mississippi River Basin (Kerr et al., 2021), and Central Asia (Zhao et al., 2006, 2013; Gillespie et al., 2008; Xu et al., 2009). However, we also note that some of these results have been challenged in subsequent literature (Gribenski et al., 2018; Miller and Andrews, 2019; Yan et al., 2023), and the notion of significant MIS 3 ice extent anywhere in the world is still debated (Dalton et al., 2022b).

A dry LGM

The early last deglaciation age we report here for a region in northeast Siberia could be linked to a lack of precipitation during the LGM compared with the preceding MIS 4/3. Indeed, lake cores at Lake Emanda and Lake El'gygytgyn both have facies typical of cold and dry climate around the peak of the global LGM around ~20 ka ago (Melles et al., 2007; Baumer et al., 2020). In addition, the El'gygytgyn core shows evidence that a period of cold and moist climate took place around the onset of MIS 4 (Melles et al., 2007). This provides support for the idea that northeast Siberia was more arid during the LGM than during MIS 3/4. LGM aridification is likely linked to the growth of the western portion of the Eurasian Ice Sheet. Some suggest that the configuration of the Eurasian Ice Sheet during LGM was blocking Atlantic moisture from traveling east (Krinner et al., 2011; Barr and Clark, 2012a). Others suggests that the configuration of the Kara and Barents Ice Sheets allowed for vast proglacial lake formation in central parts of northwest Siberia (Lambeck et al., 2006; Larsen et al., 2006; Möller et al., 2015),

https://doi.org/10.1017/qua.2025.20 Published online by Cambridge University Press

acting as an additional ephemeral moisture source for northeast Siberia during MIS 4 and 6 but not during the LGM (Krinner et al., 2011). However, the full nature of the suggested LGM aridification is not yet fully understood. Although we did not find an LGM advance in the Ambar-Yuryuyete Valley, we note that a few northeast Siberian records suggest an LGM extent nearly as large as during MIS 6–MIS 3 (Nørgaard et al., 2023), which is also partly supported by our speculative conclusions from the remote sensing. Additional dating of the glacial record in the Chersky Mountains and more broadly in northeast Siberia is still needed to further explore this question.

Conclusion

Using ^{10}Be and ^{26}Al exposure dating, we investigated the glacial history of a small valley in the Tas-Kystabyt Range of the Chersky Mountains in the central part of northeast Siberia. Based on data from two boulder and two bedrock samples, we infer that the valley was deglaciated 45.6 ± 3.4 ka ago, during the peak of MIS 3. The discrepancy between our estimate and other deglaciation ages reported throughout northeast Siberia may be explained by local variations in orography and climate, but it remains unclear whether our age is representative for the wider region or simply represents a local oddity, as we identified only one moraine within the studied valley. Our investigation provides no direct evidence for LGM ice, which is consistent with previous studies from northeast Siberia (Gualtieri et al., 2000; Glushkova, 2001; Brigham-Grette et al., 2003) although out of phase with global ice volumes that peaked at the LGM, 26–19 ka ago. Using remote sensing, we identify two generations of moraines in the Tas-Kystabyt Range toward the southwest. One generation can speculatively be linked to the dated moraine through ELA estimates, while the other generation indicating a smaller glacier remains undated but could represent the LGM ice extent.

Supplementary material. The supplementary material for this article can be found at https://doi.org/.10.1017/qua.2025.20.

Acknowledgments. We are grateful for financial support from the Independent Research Fund Denmark–Natural Sciences (grant 9040-00199B). We also thank Nastya Arzhannikova, Sergey Arzhannikov, Vladimir Tumskoy, Nikolay Torgovkin, and Daria Semikolennykh for providing valuable help during fieldwork in northeast Siberia in August–September 2021.

References

Applegate, P.J., Urban, N.M., Laabs, B.J.C., Keller, K., Alley, R.B., 2010. Modeling the statistical distributions of comsogenic exposure dates from moraines. *Geoscientific Model Development* **3**, 293–307.

Balco, G., Stone, J.O., Lifton, N.A., Dunai, T.J., 2008. A complete and easily accessible means of calculating surface exposure ages or erosion rates from ^{10}Be and ^{26}Al measurements. *Quaternary Geochronology* **3**, 174–195.

Barr, I.D., Clark, C.D., 2012a. Late Quaternary glaciations in Far NE Russia; combining moraines, topography and chronology to assess regional and global glaciation synchrony. *Quaternary Science Reviews* **53**, 72–87.

Barr, I.D., Clark, C.D., 2012b. An updated moraine map of Far NE Russia. *Journal of Maps*, **8**, 431–436.

Batchelor, C.L., Margold, M., Krapp, M., Murton, D.K., Dalton, A.S., Gibbard, P.L., Stokes, C.R., Murton, J.B., Manica, A., 2019. The configuration of Northern Hemisphere ice sheets through the Quaternary. *Nature Communications* **10**, 3713.

Baumer, M.M., Wagner, B., Meyer, H., Leicher, N., Lenz, M., Fedorov, G., Pestryakova, L.A., Melles, M., 2020. Climatic and environmental changes in the Yana Highlands of north-eastern Siberia over the lastc. 57 000 years, derived from a sediment core from Lake Emanda. *Boreas* **50**, 114–133.

Bäumler, R., Zech, W., 2000. Quaternary paleosols, tephra deposits and landscape history in South Kamchatka, Russia. *Catena* **41**, 199–215.

Benn, D.I., Lehmkuhl, F., 2000. Mass balance and equilibrium-line altitudes of glaciers in high-mountain environments. *Quaternary International* **65**, 15–29.

Bevington, P.R., Robinson, D.K., 1992. *Data Reduction and Error Analysis for the Physical Sciences*. 2nd ed. McGraw-Hill, New York.

Borchers, B., Marrero, S., Balco, G., Caffee, M., Goehring, B., Lifton, N., Nishiizumi, K., Phillips, F., Schaefer, J., Stone, J., 2016. Geological calibration of spallation production rates in the CRONUS-Earth project. *Quaternary Geochronology* **31**, 188–198.

Brigham-Grette, J., Gualtieri, L.M., Glushkova, O.Y., Hamilton, T.D., Mostoller, D., Kotov, A., 2003. Chlorine-36 and C-14 chronology support a limited last glacial maximum across central Chukotka, northeastern Siberia, and no Beringian ice sheet. *Quaternary Research* **59**, 386–398.

Corbett, L.B., Bierman, P.R., Rood, D.H., 2016. An approach for optimizing in situ cosmogenic ^{10}Be sample preparation. *Quaternary Geochronology* **33**, 24–34.

Corbett, L.B., Bierman, P.R., Caffee, M.W., Hidy, A.J., Woodruff, T.E., 2024. Quantifying replication through repeated analysis of UVM-A, a liquid reference material for cosmogenic ^{10}Be and ^{26}Al studies. *Quaternary Geochronology* **81**, 101498.

Dalton, A.S., Stokes, C.R., Batchelor, C.L., 2022a. Evolution of the Laurentide and Innuitian ice sheets prior to the Last Glacial Maximum (115 ka to 25 ka). *Earth-Science Reviews* **224**, 103875.

Dalton, A.S., Pico, T., Gowan, E.J., Clague, J.J., Forman, S.L., McMartin, I., Sarala, P., Helmens, K.F., 2022b. The marine δ^{18}O record overestimates continental ice volume during Marine Isotope Stage 3. *Global and Planetary Change* **212**, 103814.

Diekmann, B., Pestryakova, L., Nazarova, L., Subetto, D., Tarasov, P.E., Stauch, G., Thiemann, A., *et al.*, 2017. Quaternary lake dynamics in the Verkhoyansk Mountains of Eastern Siberia_implications for climate and glaciation history. *Polarforschung* **86**, 97–110.

Ehlers, J., Gibbard, P.L., 2007. The extent and chronology of Cenozoic Global Glaciation. *Quaternary International* **164–165**, 6–20.

Fabel, D., Harbor, J., 1999. The use of in-situ produced cosmogenic radionuclides in glaciology and glacial geomorphology. *Annals of Glaciology* **28**, 103–110.

Gillespie, A.R., Burke, R.M., Komatsu, G., Bayasgalan, A., 2008. Late Pleistocene glaciers in Darhad Basin, northern Mongolia. *Quaternary Research* **69**, 169–187.

Glushkova, O.Y., 2001. Geomorphological correlation of Late Pleistocene glacial complexes of Western and Eastern Beringia. *Quaternary Science Reviews* **20**, 405–417.

Gosse, J.C., Phillips, F.M., 2001. Terrestrial in situ cosmogenic nuclides: theory and application. *Quaternary Science Reviews* **20**, 1475–1560.

Gowan, E.J., Zhang, X., Khosravi, S., Rovere, A., Stocchi, P., Hughes, A.L.C., Gyllencreutz, R., Mangerud, J., Svendsen, J.I., Lohmann, G., 2021. A new global ice sheet reconstruction for the past 80 000 years. *Nature Communications* **12**, 1199.

Gribenski, N., Jansson, K.N., Preusser, F., Harbor, J.M., Stroeven, A.P., Trauerstein, M., Blomdin, R., *et al.*, 2018. Re-evaluation of MIS 3 glaciation using cosmogenic radionuclide and single grain luminescence ages, Kanas Valley, Chinese Altai. *Journal of Quaternary Science* **33**, 55–67.

Gualtieri, L., Glushkova, O.Y., Brigham-Grette, J., 2000. Evidence for restricted ice extent during the last glacial maximum in the Koryak Mountains of Chukotka, far eastern Russia. *GSA Bulletin* **112**, 1106–1118.

Halsted, C.T., Bierman, P.R., Shakun, J.D., Davis, P.T., Corbett, L.B., Drebber, J.S., Ridge, J.C., 2024. A critical re-analysis of constraints on the timing and rate of Laurentide Ice Sheet recession in the northeastern United States. *Journal of Quaternary Science* **39**, 54–69.

Heyman, J., Stroeven, A.P., Harbor, J.M., Caffee, M.W., 2011. Too young or too old: Evaluating cosmogenic exposure dating based on analysis of compiled boulder exposure ages. *Earth and Planetary Science Letters* **302**, 71–80.

Hughes, P.D., Gibbard, P.L., Ehlers, J., 2013. Timing of glaciation during the last glacial cycle: evaluating the concept of a global "Last Glacial Maximum" (LGM). *Earth-Science Reviews* **125**, 171–198.

Kerr, P.J., Tassier-Surine, S.A., Kilgore, S.M., Bettis, E.A. III, Dorale, J.A., Cramer, B.D., 2021. Timing, provenance, and implications of two MIS 3 advances of the Laurentide Ice Sheet into the Upper Mississippi River Basin, USA. *Quaternary Science Reviews* **261**, 106926.

Kohl, C.P., Nishiizumi, K., 1992. Chemical isolation of quartz for measurement of in-situ-produced cosmogenic nuclides. *Geochimica et Cosmochimica Acta* **56**, 3583–3587.

Krinner, G., Diekmann, B., Colleoni, F., Stauch, G., 2011. Global, regional and local scale factors determining glaciation extent in Eastern Siberia over the last 140,000 years. *Quaternary Science Reviews* **30**, 821–831.

Lambeck, K., Purcell, A., Funder, S., KjaeR, K.H., Larsen, E., Moller, P.E.R., 2006. Constraints on the Late Saalian to early Middle Weichselian ice sheet of Eurasia from field data and rebound modelling. *Boreas* **35**, 539–575.

Larsen, E., KjaeR, K.H., Demidov, I.N., Funder, S., Grøsfjeld, K., Houmark-Nielsen, M., Jensen, M., Linge, H., Lysa, A., 2006. Late Pleistocene glacial and lake history of northwestern Russia. *Boreas* **35**, 394–424.

Lifton, N., Sato, T., Dunai, T.J., 2014. Scaling in situ cosmogenic nuclide production rates using analytical approximations to atmospheric cosmic-ray fluxes. *Earth and Planetary Science Letters* **386**, 149–160.

Lisiecki, L.E., Raymo, M.E., 2005. A Pliocene-Pleistocene stack of 57 globally distributed benthic $\delta^{18}O$ records. *Paleoceanography* 20. https://doi.org/10.1029/2004pa001071.

Mangerud, J., Gyllencreutz, R., Lohne, Ø., Svendsen, J.I., 2011. Glacial history of Norway. In: Ehlers, J., Gibbard, P.L., Hughes, P.D. (Eds.), *Quaternary Glaciations—Extent and Chronology: A Closer Look*. Developments in Quaternary Science, Vol. **15**. Elsevier Science and Technology, Amsterdam, pp. 279–98.

Melles, M., Brigham-Grette, J., Glushkova, O.Y., Minyuk, P.S., Nowaczyk, N.R., Hubberten, H.-W., 2007. Sedimentary geochemistry of core PG1351 from Lake El'gygytgyn—a sensitive record of climate variability in the East Siberian Arctic during the past three glacial–interglacial cycles. *Journal of Paleolimnology* **37**, 89–104.

Miller, G.H., Andrews, J.T., 2019. Hudson Bay was not deglaciated during MIS-3, *Quaternary Science Reviews* **225**, 105944.

Möller, P., Alexanderson, H., Funder, S., Hjort, C., 2015. The Taimyr Peninsula and the Severnaya Zemlya archipelago, Arctic Russia: a synthesis of glacial history and palaeo-environmental change during the Last Glacial cycle (MIS 5e–2). *Quaternary Science Reviews* **107**, 149–181.

Nishiizumi, K., 2004. Preparation of 26Al AMS standards. *Nuclear Instruments and Methods in Physics Research Section B: Beam Interactions with Materials and Atoms* **223–224**, 388–392.

Nishiizumi, K., Imamura, M., Caffee, M.W., Southon, J.R., Finkel, R.C., McAninch, J., 2007. Absolute calibration of ^{10}Be AMS standards. *Nuclear Instruments and Methods in Physics Research Section B: Beam Interactions with Materials and Atoms* **258**, 403–413.

Nørgaard, J., Margold, M., Jansen, J.D., Kurbanov, R., Szuman, I., Andersen, J.L., Olsen, J., Faurschou Knudsen, M., 2023. Absence of large-scale ice masses in central northeast Siberia during the late Pleistocene. *Geophysical Research Letters* **50**, e2023GL103594.

Porter, C., Morin, P., Howat, I., Noh, M.-J., Bates, B., Peterman, K., Keesey, S., *et al.*, 2018. ArcticDEM, Version 3. Harvard Dataverse, V1. https://doi.org/10.7910/DVN/OHHUKH.

Salonen, V-P., Moreau, J., Hyttinen, O., Eskola, K.O., 2014. Mid-Weichselian interstadial in Kolari, western Finnish Lapland. *Boreas* **43**, 627–638.

Seidenkrantz, M.S., Kuijpers, A., Olsen, J., Pearce, C., Lindblom, S., Ploug, J., Przybyło, P., Snowball, I., 2019. Southwest Greenland shelf glaciation during MIS 4 more extensive than during the Last Glacial Maximum. *Scientific Reports* **9**, 15617.

Simms, A.R., Lisiecki, L., Gebbie, G., Whitehouse, P.L., Clark, J.F., 2019. Balancing the last glacial maximum (LGM) sea-level budget. *Quaternary Science Reviews* **205**, 143–153.

Søndergaard, A.S., Larsen, N.K., Steinemann, O., Olsen, J., Funder, S., Egholm, D.L., Kjær, K.H., 2020. Glacial history of Inglefield Land, north Greenland from combined 10Be and in-situ 14C exposure dating. *Climate of the Past* **16**, 1999–2015.

Stauch, G., Gualtieri, L., 2008. Late Quaternary glaciations in northeastern Russia. *Journal of Quaternary Science* **23**, 545–558.

Stauch, G., Lehmkuhl, F., 2010. Quaternary glaciations in the Verkhoyansk Mountains, Northeast Siberia. *Quaternary Research* **74**, 145–155.

Stauch, G., Lehmkuhl, F., Frechen, M., 2007. Luminescence chronology from the Verkhoyansk Mountains (North-Eastern Siberia). *Quaternary Geochronology* **2**, 255–259.

Stokes, C.R., Tarasov, L., Dyke, A.S., 2012. Dynamics of the North American Ice Sheet Complex during its inception and build-up to the Last Glacial Maximum. *Quaternary Science Reviews* **50**, 86–104.

Svendsen, J.I., Alexanderson, H., Astakhov, V.I., Demidov, I., Dowdeswell, J.A., Funder, S., Gataullin, V., *et al.*, 2004. Late Quaternary ice sheet history of northern Eurasia. *Quaternary Science Reviews* **23**, 1229–1271.

Ward, B.C., Bond, J.D., Gosse, J.C., 2007. Evidence for a 55–50 ka (early Wisconsin) glaciation of the Cordilleran ice sheet, Yukon Territory, Canada. *Quaternary Research* **68**, 141–150.

Xu, X., Yang, J., Dong, G., Wang, L., Miller, L., 2009. OSL dating of glacier extent during the Last Glacial and the Kanas Lake basin formation in Kanas River valley, Altai Mountains, China. *Geomorphology* **112**, 306–317.

Yan, Q., Owen, L.A., Guo, C., Zhang, Z., Zhang, J., Wang, H., 2023. Widespread glacier advances across the Tian Shan during Marine Isotope Stage 3 not supported by climate-glaciation simulations. *Fundamental Research* **3**, 102–110.

Zech, W., Zech, R., Zech, M., Leiber, K., Dippold, M., Frechen, M., Bussert, R., Andreev, A., 2011. Obliquity forcing of Quaternary glaciation and environmental changes in NE Siberia. *Quaternary International* **234**, 133–145.

Zhao, J., Yin, X., Harbor, J.M., Lai, Z., Liu, S., Li, Z., 2013. Quaternary glacial chronology of the Kanas River valley, Altai Mountains, China. *Quaternary International* **311**, 44–53.

Zhao, J., Zhou, S., He, Y., Ye, Y., Liu, S., 2006. ESR dating of glacial tills and glaciations in the Urumqi River headwaters, Tianshan Mountains, China. *Quaternary International* **144**, 61–67.

https://doi.org/10.1017/qua.2025.20 Published online by Cambridge University Press